Soil Dynamics and Earthquake Engineering 168 (2023) 107835

Contents lists available at ScienceDirect

Soil Dynamics and Earthquake Engineering

journal homepage: www.elsevier.com/locate/soildyn

Performance-based seismic assessment of slope systems

Jonathan D. Bray [a,*], Jorge Macedo [b]

[a] University of California, Berkeley, CA, 94702-1710, USA
[b] Georgia Institute of Technology, Atlanta, GA, USA

ARTICLE INFO

Keywords:
Dam
Displacement
Earthquake
Hazard
Performance
Probabilistic
Slope

ABSTRACT

The calculated seismic slope displacement provides a valuable index of the seismic performance of earth embankments and natural slopes. Sliding block models are often employed. The specific features of each sliding block method determine its reliability. Rigid sliding block models should not be used except for the limited case when the sliding mass is rigid. A coupled nonlinear deformable stick-slip sliding block model calculates reasonable seismic slope displacements. The primary source of uncertainty in assessing the seismic performance of an earth slope is the input ground motion. Hence, many ground motion records for each tectonic setting should be employed. Seismic slope displacement depends primarily on the earth structure's yield coefficient and the earthquake ground motion's spectral acceleration at the effective fundamental period of the sliding mass. Coupled nonlinear sliding block models enable the sensitivity of the seismic slope displacement and its uncertainty to key input parameters to be assessed. These procedures can be implemented within a performance-based design framework to estimate the seismic slope displacement hazard, which is a more rational approach.

1. Introduction

The failure of slope systems (e.g., earth dams, waste fills, natural slopes) during an earthquake can produce significant losses. Additionally, major damage without failure can have severe economic consequences. Accordingly, the seismic performance of earth structures and natural slopes requires evaluation. The assessment of the seismic performance of slope systems ranges from using straightforward pseudo-static procedures to advanced nonlinear effective stress finite difference analyses. Performance should be evaluated through an assessment of the potential for seismically induced permanent displacement. A modified Newmark [1] sliding block analysis is often employed as part of the seismic evaluation of earth structures and natural slopes. They provide a preliminary assessment of an earth system's seismic performance. However, the available simplified seismic slope displacement procedures differ significantly in important ways, which should be considered before using them in engineering practice. Key aspects of these procedures are critiqued in this paper, and recently developed procedures by the authors for estimating earthquake-induced shear deformation in earth and waste structures and natural slopes are summarized. These probabilistic seismic slope displacement methods are implemented within a performance-based framework using a seismic slope displacement hazard calculation. Recommendations for the use of seismic slope displacement procedures in engineering practice are shared.

2. Seismic slope stability analysis

2.1. Critical design issues

Two critical design issues must be addressed when evaluating the seismic performance of an earth structure or slope.

1. Most importantly, the engineer must investigate if there are materials in the structure or its foundation that will lose significant strength due to cyclic loading (e.g., liquefaction). If severe strength loss is possible, this issue should be the primary focus of the evaluation because a flow slide could occur. The post-cyclic strength of materials that lose strength due to earthquake loading must be evaluated. The post-cyclic static slope stability factor of safety (*FS*) should be calculated. If it is near to or below one, a flow slide is possible, such as the tailings dam flow failure shown in Fig. 1. Mitigation measures or advanced analyses are warranted to address or to evaluate the flow slide and its consequences.
2. If materials within or below the earth structure will not lose significant strength due to cyclic loading, the deformation of the earth structure or slope must be evaluated to assess if earthquake-induced

* Corresponding author.
E-mail address: jonbray@berkeley.edu (J.D. Bray).

https://doi.org/10.1016/j.soildyn.2023.107835
Received 26 November 2022; Received in revised form 10 February 2023; Accepted 10 February 2023
Available online 26 February 2023

deformation adversely affects the performance of the system. The estimation of seismically induced slope displacement helps the engineer address this issue in combination with nonlinear effective stress finite different analyses when warranted. The calculation of seismic slope displacement using deformable sliding block analyses are the focus of this paper.

2.2. Shear-induced seismic displacement

The calculated seismic slope displacement from a modified Newmark [1] procedure, whether it is simplified or advanced, is an index of the potential seismic performance of the earth structure or slope. Seismic slope displacement estimates are approximate in nature due to the complexities of the dynamic response of the earth/waste materials involved and the variability of the earthquake ground motion, among other factors. However, when viewed as an index of potential seismic performance, the calculated seismic slope displacement can be used effectively in engineering practice to evaluate the seismic stability of earth structures and natural slopes.

A modified Newmark sliding block model can capture that part of the seismically induced permanent displacement attributed to shear deformation (i.e., either rigid body slippage along a distinct failure surface or distributed shearing within the deformable sliding mass). Ground movement due to volumetric compression of the soil is not captured explicitly by Newmark models. The top of a slope can displace downward due to shear deformation or volumetric compression of the slope materials. However, movements at the top of a slope resulting from distributed shear straining within the sliding mass or stick-slip sliding along a failure surface are mechanistically different from top-of-slope movements that result from seismically induced volumetric compression of the materials forming the slope.

Although a Newmark-type procedure may appear to capture the overall top-of-slope displacement for cases where seismic compression due to volumetric contraction of soil or waste is the dominant mechanism, this is merely because the seismic inertial forces that produce large shear strains often produce correspondingly large volumetric compression strains. This apparent correspondence does not imply that a Newmark sliding block model should be used to estimate seismic displacement due to volumetric strain. There are cases where the Newmark method does not capture the overall displacement at the top of a slope, such as the seismic compression of compacted earth fills (e.g., Ref. [3]). There are other cases when there are negligible volumetric-induced slope movements such as in the short-term undrained response of a saturated clay slope. Shear-induced deformation and volumetric-induced deformation should be analyzed separately using procedures based on the sliding block model to estimate shear-induced displacement and using other procedures to estimate volumetric-induced displacement (e.g., Ref. [4]). The combined effects of the shear-induced ground movements and volumetric-induced ground movements should then be evaluated.

3. Seismic slope displacement procedures

3.1. General

The critical components of a sliding block analysis are: 1) the dynamic resistance of the structure, 2) the earthquake ground motion, 3) the dynamic response of the sliding mass, and 4) the permanent displacement calculational procedure. The dynamic resistance of the earth/waste structure or natural slope is a key component in the analysis. The system's yield coefficient defines its maximum dynamic resistance. The earthquake ground motion is the input to assessing the seismic demand on the system. The dynamic response of the potential sliding mass to the input earthquake ground motion should be considered because the sliding mass is rarely rigid. The sliding block calculational procedure should capture the coupled dynamic response and sliding resistance of the sliding mass during ground shaking. Other factors, such as topographic effects, can be important in some cases. In critiquing a seismic slope displacement procedure, one should consider how each procedure characterizes the slope's dynamic resistance, the earthquake ground motion, the dynamic response of the system to the ground motion, and the calculational procedure.

3.2. Dynamic resistance

The slope's yield coefficient (k_y) represents its dynamic resistance. It is calculated as the horizontal seismic coefficient that results in a $FS = 1.0$ in a pseudostatic slope stability analysis. It depends primarily on the dynamic strength of the material along the critical sliding surface, the structure's geometry and weight, and the initial pore water pressures that determine the in situ effective stress within the system. The yield coefficient greatly influences the seismic slope displacement calculated by any Newmark-type sliding block model.

The primary issue in calculating k_y is estimating the dynamic strength of the critical strata within the slope. Several publications include extensive discussions of the dynamic strength of soil (e.g., Refs. [5,6,7]). The engineer should devote considerable attention and resources to developing realistic estimates of the dynamic strengths of key slope materials. Effective stress, drained strength parameters are appropriate for unsaturated or dilative cohesionless soil. Pore water pressure generation or undrained strength parameters and post-cyclic residual shear strength are required to characterize saturated, contractive cohesionless soil. Newmark procedures should not be applied to cases involving soil that undergoes severe strength loss due to earthquake shaking (e.g., liquefaction) without considerable judgment. For clay soil that does not liquefy, its dynamic peak undrained shear strength ($s_{u,dyn,peak}$) can be related to its static peak undrained shear strength ($s_{u,stat,peak}$) using adjustment factors [8,9] as:

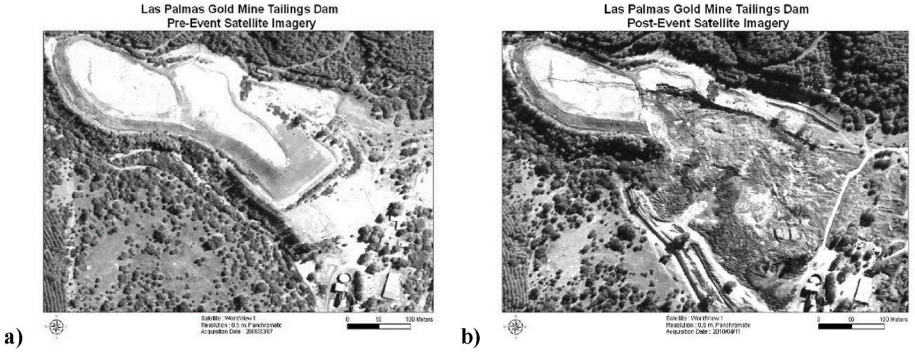

Fig. 1. (a) Pre-earthquake and (b) post-earthquake satellite images of the Las Palmas Gold Mine Tailings Dam failure due to a liquefaction-induced flow failure during the 2010 Maule, Chile earthquake [2].

$$s_{u,dyn,peak} = s_{u,stat,peak}\,(C_{rate})(C_{cyc})(C_{prog})(C_{def}) \quad (1)$$

where C_{rate} = rate of loading factor, C_{cyc} = cyclic degradation factor, C_{prog} = progressive failure factor, and C_{def} = distributed shear deformation factor.

The shear strength of a plastic clay increases as the rate of loading increases (e.g., Refs. [7,10–12]). The undrained shear strength of viscous clay materials can increase by about 10%–15% for each ten-fold increase in the strain rate. For example, Biscontin and Pestana [12] found that $s_{u,dyn,peak}$ at earthquake rate of loadings was 1.3x larger than $s_{u,stat,peak}$ measured at conventional rates of loading in the vane shear test in a soft plastic clay. Rau [13] found the shear strength mobilized in the first cycle of a rapid cyclic simple shear test on San Francisco Young Bay Mud from Hamilton Air Force Base was up to 40%–50% higher than that mobilized in a conventional static test performed at typical loading rates. Cyclic simple shear tests on Young Bay Mud at the San Francisco-Oakland Bay Bridge [14] indicated the strength mobilized in the first cycle of loading was about 40% greater than that mobilized in the monotonic test at the conventional strain-rate for monotonic shear tests at the same level of strain. It depends on the clay and testing device, etc., but generally, the ratio of $s_{u,dyn,peak}/s_{u,stat,peak}$ in one cycle of loading at a strain rate representative of an earthquake loading relative to that for a conventional static test leads to a C_{rate} value on the order of 1.3–1.7.

With additional cycles of loading, the peak undrained shear strength of a plastic clay can degrade (e.g., Ref. [10]). This effect is captured with the cyclic degradation factor: C_{cyc}. For example, Rau [13] found that by the 15th load cycle, the cyclic shear strength of San Francisco Young Bay Mud had reduced from its highest value in the first cycle of rapid loading to a value close to that obtained in the static tests. With more cycles of loading its strength could reduce further. Shear strength reductions of 10%–30%, which are equivalent to C_{cyc} = 0.9 to 0.7, might be appropriate for strain-softening clay shaken by a large magnitude earthquake with many cycles of loading. Due to cyclic degradation, as the number of cycles of loading increases, a strain-softening clay's dynamic shear strength decreases, especially if the volumetric threshold strain [15] of the material is exceeded, shear strains approach or exceed values that are half of its failure strain, and stress reversals occur.

The increased rate of loading during earthquake shaking increases the dynamic peak shear strength of a plastic clay while a larger number of load cycles reduces its dynamic peak shear strength due to cyclic degradation. For example, Rumpelt and Sitar [16] found San Francisco Young Bay Mud's post-cyclic peak undrained shear strength ratio (s_u/σ'_{vo}) measured at slow strain-rates was about equal to its pre-seismic static strength of s_u/σ'_{vo} = 0.35. However, its s_u/σ'_{vo} was 0.55 for 2 cycles of rapid stress-controlled loading (an increase of 1.6), 0.44–0.48 for 12 load cycles (an increase of 1.3), and 0.41 for 22 load cycles (an increase of 1.2).

In addition to the rate of loading and cyclic degradation factors, a progressive failure factor of less than one should be applied if the clay exhibits significant post-peak strain softening when it is likely that the dynamic peak shear strength will not be mobilized along the entire failure surface at the same time [9]. This progressive failure phenomenon can be captured in rigid-perfectly plastic limit equilibrium slope stability analysis through the use of a reduced "average" shear strength of the clay along the sliding surface. A value of C_{prog} = 0.9 is often appropriate for moderately sensitive plastic clay.

Additionally, significant shear deformation can accumulate within part of the potential sliding mass for stress cycles slightly less than the dynamic peak shear strength due to the nonlinear elastoplastic response of soil [8,51]. This additional shear deformation initiates before the localized sliding surface develops fully. It continues due to the general shearing of soil distributed over a zone that is considerably thicker than that of the localized sliding surface after it fully develops. This additional shear-induced displacement is denoted as distributed shear deformation. A value of C_{def} = 0.9 is often appropriate to capture approximately this effect in a clay slope in a Newmark sliding block analysis.

Therefore, the dynamic peak shear strength of a plastic clay used in a sliding block analysis should depend on the combined effects of the rapid rate of earthquake loading and the number of significant cycles of loading, as well as the progressive failure and deformable sliding block effects. For example, if only one cycle of a near-fault, forward-directivity pulse motion occurs, the dynamic peak shear strength of San Francisco Young Bay Mud might be 40% higher than its static peak shear strength due to the combined effect of C_{rate} = 1.4 and C_{cyc} = 1.0. Conversely, if 30 cycles of loading are applied from a backwards-directivity long duration motion, the clay's dynamic peak strength might only be 10% greater than its static peak shear strength due to the combined effect of C_{rate} = 1.4 and C_{cyc} = 0.8. Combining these factors in Eq. (1) and including progressive failure and deformable sliding block effects produces $s_{u,dyn,peak}/s_{u,stat,peak}$ ratios of (1.4)(1.0)(0.9)(0.9) = 1.1 for the forward-directivity single pulse motion and (1.4)(0.8)(0.9)(0.9) = 0.9 for the backward-directivity multiple load cycles motion. As the shear strength of clay depends on the characteristics of the earthquake loading, one should use different dynamic peak shear strengths for the clay depending primarily on the number of significant load cycles of the earthquake ground motion.

The use of a clay's dynamic peak shear strength would only be appropriate for a strain-hardening material or when limited seismic slope displacement is calculated. If moderate-to-large seismic slope displacement is calculated for the case when the clay exhibits strain-softening, the dynamic shear strength used in the sliding block analysis needs to be adjusted to be compatible with the amount of shear strain induced in the clay (e.g., Ref. [17]). As the dynamic shear strength reduces as the clay is deformed beyond its peak shear strength, the resulting yield coefficient will reduce, and additional seismic slope displacement will be calculated. It is unconservative to use a constant k_y value based on peak shear strength when the soil exhibits strain-softening. If a large displacement is calculated, the clay's residual shear strength is appropriate for calculating k_y. The residual shear strength of clay is often found to be insensitive to variations in strain-rate (e.g. Ref. [12]), so its dynamic residual shear strength can be assumed to be equal to its static residual shear strength.

Duncan [18] found consistent estimates of a slope's static *FS* are calculated if a slope stability procedure that satisfies all three conditions of equilibrium is employed. Computer programs that utilize methods that satisfy full equilibrium, such as the Spencer, Morgenstern and Price, and Generalized Janbu methods, should be used to calculate the static *FS*. These methods should also be used to calculate k_y.

Lastly, the potential sliding mass that has the lowest static *FS* may not be the most critical for dynamic analysis. A search should be made to find sliding surfaces that produce low k_y values as well. The most important parameter for identifying critical potential sliding masses for dynamic problems is finding the sliding surface with the lowest k_y/k_{max} value, where k_{max} is an estimate of the maximum seismic loading considering the dynamic response of the sliding mass.

3.3. Earthquake ground motion

An acceleration-time history provides a complete characterization of an earthquake ground motion. In a simplified description of a ground motion, its intensity, frequency content, and duration must be specified at a minimum. In this manner, a ground motion can be described in terms of parameters such as peak ground acceleration (*PGA*), mean period (T_m), and significant duration ($D_{5\text{-}95}$). It is overly simplistic to characterize an earthquake ground motion by just its *PGA*, because ground motions with identical *PGA* values can vary significantly in terms of frequency content and duration and, most importantly, in terms of their effects on seismic slope performance.

The use of *PGA* as the seismic intensity parameter in a seismic slope displacement procedure indicates a rigid sliding block model has been

employed. Doing so ignores the dynamic response of the potential sliding mass, which is important for cases when the sliding mass cannot be assumed to be infinitely stiff. The Makdisi and Seed [19] method modifies the *PGA* estimated at the crest of a dam or slope (PGA_{crest}) to capture the dynamic response of the potential sliding mass using the equivalent-acceleration concept described in Ref. [20]. However, estimating the maximum seismic demand on an earth embankment (k_{max}) as a function of PGA_{crest} is problematic because it is highly uncertain to estimate the *PGA* that is produced at the top of a dam or slope during earthquake shaking. Alternatively, the 5%-damped elastic spectral acceleration (S_a) at the degraded fundamental period of the potential sliding mass, which occurs in the material below the potential sliding mass assuming it is outcropping, can be used as the seismic intensity parameter.

Spectral acceleration has been commonly employed in earthquake engineering to characterize an equivalent seismic loading on a structure from the earthquake ground motion. Bray and Travasarou [21] found that S_a at the degraded fundamental period of the potential sliding mass for the material below it was the optimal ground motion intensity measure in terms of efficiency and sufficiency (i.e., it minimizes the variability in its correlation with seismic displacement, and it renders the relationship independent of other variables, respectively, [22]). An estimate of the initial fundamental period of the sliding mass (T_s) is required when using spectral acceleration. T_s is useful because it represents the dynamic response characteristics of a sliding mass. Additional benefits of using S_a are it can be estimated reliably with ground motion models, and it is available at various return periods in ground motion hazard maps. Spectral acceleration captures the intensity and frequency content characteristics of an earthquake motion, but it fails to capture duration. Moment magnitude (M_w) can be added to capture the duration of strong shaking. Some Newmark-type models (e.g., Ref. [23]; and [24]) also use peak ground velocity (*PGV*) to bring in frequency content or near-fault forward-directivity effects.

Ground motion characteristics vary systematically in different tectonic settings. For instance, the NGAWest-2 ground motion models (GMMs) differ significantly from the NGA-Sub GMMs for subduction interface and intraslab earthquakes (e.g., Refs. [25,26]; respectively). Hence, it is important to use suites of a sufficient number of ground motion records appropriate for the tectonic settings affecting the project. It follows that seismic slope displacement procedures for use with shallow crustal earthquakes along active plate margins, subduction zone interface and intraslab earthquakes, and stable continental earthquakes will differ. As significant regional distinctions are identified (e.g., crustal attention in Japan vs. South America for subduction zone interface earthquakes), additional refinements may be justified. The exponential growth of the number of ground motion records in different regions of each tectonic setting is enabling researchers to examine these issues.

3.4. Dynamic response and seismic displacement calculation

The seismic slope displacement depends on the dynamic response of the potential sliding mass. With all other factors held constant, seismic displacement increases when the sliding mass is near resonance compared to that calculated for very stiff or very flexible slopes (e.g., Refs. [27–29]). Many of the available seismic slope displacement procedures employ the original Newmark [1] rigid sliding block assumption. These procedures do not capture the dynamic response of the deformable sliding mass during earthquake shaking. Thus, seismic slope procedures based on the rigid block model should not be used in cases when the ground cannot be assumed to be rigid. Rigid sliding block models are only appropriate for shallow sliding of very stiff materials.

Seed and Martin [20] introduced the concept of an average acceleration to represent the seismic loading of a sliding earth mass. When applied to a rigid sliding mass, the average acceleration-time history produces the same dynamic shear stresses along the sliding surface that is produced when a dynamic analysis of the deformable earth structure is performed. The calculation of the average acceleration-time history in a dynamic analysis that assumes no relative displacement occurs along the failure surface is decoupled from the rigid sliding block calculation that is performed using the average acceleration-time history to calculate the seismic slope displacement. Given the large sources of uncertainty present in some analyses, the decoupled approximation is often judged to provide a reasonable estimate of seismic slope displacement (e.g., [28,53]). However, it is not always reasonable, and it can lead to significant overestimation near resonance and some level of underestimation for cases where the structure has a large fundamental period or the ground motion is an intense near-fault motion. A nonlinear coupled stick-slip deformable sliding block model offers a more realistic representation of the dynamic response of an earth system by accounting for the deformability of the sliding mass and by considering the simultaneous occurrence of its nonlinear dynamic response and periodic sliding episodes (Fig. 2). Its validation with shaking table experiments provides confidence in its use [29].

For seismic slope displacement methods that incorporate the seismic response of a deformable sliding block, the initial fundamental period of the sliding mass (T_s) of a relatively long sliding mass can be estimated as: $T_s = 4H/V_s'$, where H is the maximum height of the sliding mass and V_s' is its equivalent shear wave velocity $= \Sigma[(V_{si})(m_i)]/\Sigma(m_i)$, where m_i is each differential mass i with shear wave velocity of V_{si} [31]. For the case of a triangular-shaped sliding mass, $T_s = 2.6H/V_s'$ should be used [32]. The initial fundamental period of the sliding mass can be estimated approximately for other cases using a mass-weighted fundamental period (T_s') of rectangular slices of the sliding mass, as illustrated in Fig. 3. T_s' is calculated as the mass-weighted fundamental period of each incremental slice of the sliding mass, wherein the fundamental period of each rectangular slice of height H_i and shear wave velocity of V_{si}' is calculated as $T_{si} = 4\,H_i/V_{si}'$. The effective height of the entire slide mass (H') is calculated as $(T_s')(V_s')/4$, and the initial fundamental period of the sliding mass can be approximated as $T_s = 4\,H'/V_s'$. H' varies from 0.65 H to 1.0 H, where H is the maximum height of a vertical line within the sliding mass (not the total height of the sliding mass from its base to its top). The use of T_s implicitly assumes the material below the sliding mass is rigid. Adjustments may be required if the base is not stiff relative to the potential sliding mass or if topographic effects are significant. As the method is based on 1D analysis, which may underestimate the seismic demand of shallow sliding at the top of 2D systems affected by topographic amplification, the input motion's intensity parameter should be amplified by 25% for moderately steep slopes and by 50% for steep slopes [21]. It may be amplified by 100% for localized sliding at the dam crest [33]. Lastly, the effects of two-way sliding and vertical ground motions can be neglected in most cases [17]. However, as stated previously, the yield coefficient should be compatible with the dynamic shear strength of the soil, which can vary during sliding due to cyclic degradation and strain-softening.

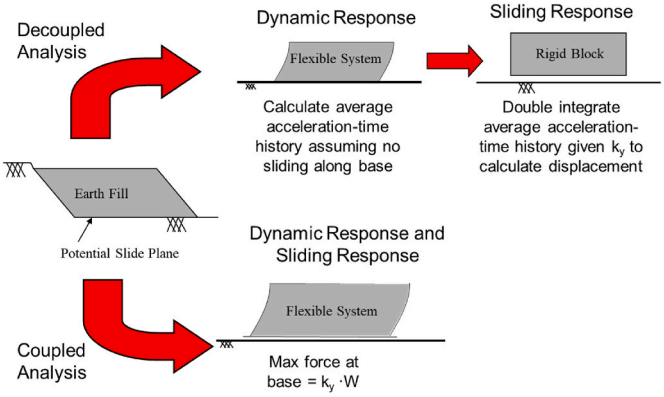

Fig. 2. Decoupled and fully coupled sliding block analysis [30].

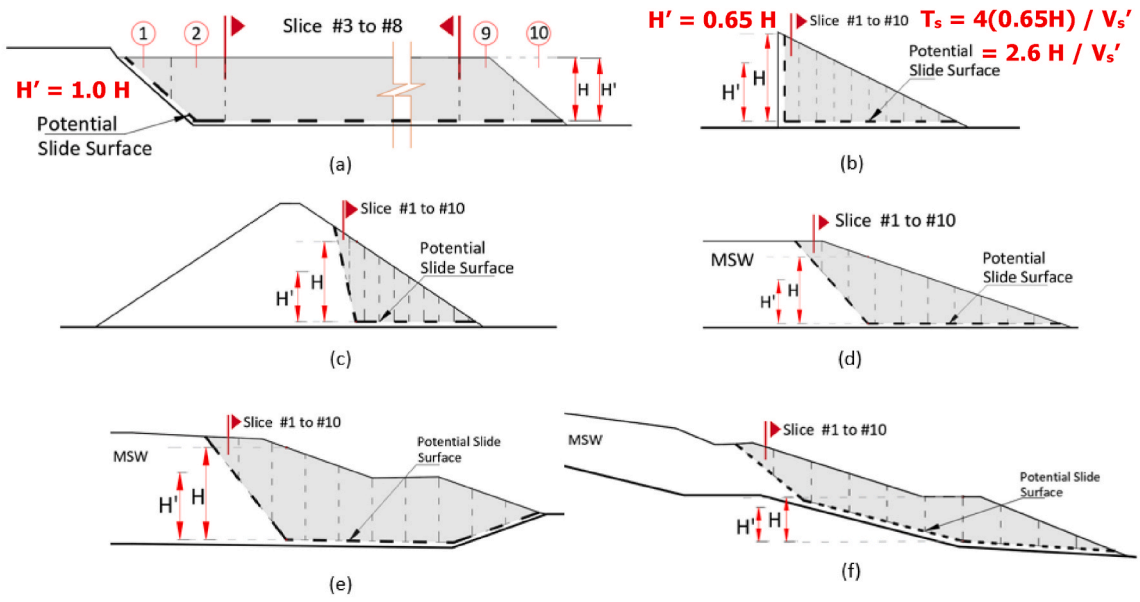

Example calculation of H' for Case d

Slice #	Height, H_i (m)	Width, W_i (m)	Slice Area, A_i (m^2)	Vs_i (m/s)	$(Vs_i) \times (A_i)$	Ts_i (s)	$(Ts_i) \times (A_i)$
1	8.85	15.30	137.9	300.0	41,370	0.118	16.27
2	23.95	15.30	373.3	300.0	111,990	0.319	119.2
3	33.75	15.30	554.0	300.0	166,200	0.450	249.3
4	34.65	15.30	539.0	300.0	161,700	0.462	249.0
5	29.35	15.30	456.1	300.0	136,830	0.391	178.5
6	24.00	15.30	373.2	300.0	111,960	0.320	119.4
7	18.65	15.30	290.2	300.0	87,060	0.249	72.26
8	13.35	15.30	207.3	300.0	62,190	0.178	36.90
9	8.00	15.30	124.4	300.0	37,320	0.107	13.27
10	2.65	15.30	41.5	300.0	12,450	0.035	1.47
Max height in slide mass, H = 37.3 m			**ΣA_i** = 3,097 m^2		**$\Sigma (V_{si} \times A_i)$** = 929,100 m^3/s		**$\Sigma (T_{si} \times A_i)$** = 1,056 $m^2 s$
$V_{s,av} = \Sigma (V_{si} \times A_i) / \Sigma A_i$ = 300.0 m/s					**$T_{s,av} = \Sigma (T_{si} \times A_i) / \Sigma A_i$** = 0.341 s		
H' = $T_{s,av} \times V_{s,av}$ / 4.0 = (0.341 s)(300.0 m/s) / 4.0 = 25.58 m					**H' = (25.58 m / 37.3 m) H** = 0.69 H		

Fig. 3. Estimating the initial fundamental period of potential sliding blocks using $T_s = 4\ H'/V_s'$ (after [31].

3.5. Summary of seismic slope displacement procedures

Key characteristics of a few of the widely used simplified seismic slope displacement procedures are summarized in Table 1. As discussed later, the Bray and Macedo [24] procedure is an update to the Bray and Travasarou [21] procedure which takes advantage of an order of magnitude increase in the number of ground motion records from shallow crustal earthquakes, so the latter procedure is not included in Table 1. Likewise, the Macedo et al. [34] procedure is an update of the Bray et al. [36] procedure of subduction zone interface earthquakes, and Macedo et al. [34] introduce a separate model for subduction zone intraslab earthquakes because they differ significantly from interface earthquakes.

The Makdisi and Seed [19] procedure is based on a limited number of analyses using only 4 ground motion records, one of which was created by combining parts of the other 3 records because records from large magnitude earthquakes were not available at the time of its development. The Jibson [52] method is only applicable to rigid sliding masses. The [23,24]; and [34] procedures are strictly only applicable to a sliding mass whose response is dominated by its 1D response. However, as discussed previously, much of the response of 2D systems can be captured reasonably well by its 1D dynamic response, and the 1D results can be adjusted if 2D effects are judged to be important. The value of using 1D analysis is that the important influence of the input ground motion can be considered using thousands of ground motion records. In this paper, the Bray and Macedo and Macedo et al. [24,34] seismic slope displacement procedures are summarized and applied to develop a probabilistic seismic displacement hazard curve to enable a

Table 1
Summary of key characteristics of some seismic slope displacement procedures.

Characteristic	Makdisi & Seed 1978. [19]	Jibson 2007 [52]	Rathje & Antonakos. [23]	Bray & Macedo 2019. [24]	Macedo et al. 2023. [34]
Tectonic Setting	Shallow Crustal	Shallow Crustal	Shallow Crustal	Shallow Crustal	Subduction Zone Interface & Intraslab
# of records	4	875	2383 (400)[1]	6711	6240 & 8299
# of analyses	21	875	14,000 (1600)[1]	2,900,000	1,510,000 & 1,856,000
Resistance	Constant k_y	Constant k_y	Constant k_y	Constant k_y	Constant k_y
Sliding mass	Flexible	Rigid	Flexible & Rigid	Flexible & Rigid	Flexible & Rigid
Calculation	Decoupled	Newmark	Coupled	Coupled	Coupled
Foundation	Rigid	Rigid	Rigid	Rigid	Rigid
Seismic Intensity Parameters	PGA_{crest}, M_w	PGA, M_w	PGA, PGV, T_s, T_m^2	$Sa(1.3T_s)$, T_s, M_w, PGV FD motion	$Sa(1.3T_s)$, T_s, M_w, PGV optional
Uncertainty	Deterministic	Probabilistic	Probabilistic	Probabilistic	Probabilistic

Notes: 1. Number of records and analyses based on [35] and values in parenthesis are additional analyses performed in [23].
2. T_s is the period of the sliding mass and T_m is mean period of the input motion.

performance-based assessment.

4. Performance-based seismic slope displacement procedures

4.1. General

The characteristics of the input ground motion are a key source of uncertainty in the estimate of seismic slope displacement. Thus, it is prudent to employ a comprehensive database of ground motion records for the tectonic setting of the governing earthquakes. Recently developed seismic slope procedures for shallow crustal earthquakes and for interface events and intraslab events in subduction earthquake zones are summarized in this section of the paper.

In these procedures, seismic slope displacement is modeled as a mixed random variable with a certain probability mass at zero displacement and a probability density for finite displacement values [21]. This approach allows the regression of seismic slope displacements (D) to not be controlled by meaningless values of calculated seismic displacement (i.e., $D < 0.5$ cm). The probability density function of seismic displacements is:

$$f_D(d) = \overline{P}\delta(d - d_0) + (1 - \overline{P})\overline{f}_D(d) \tag{2}$$

where $f_D(d)$ is the displacement probability density function; $\overline{P}$ is the probability mass at $D = d_0$; $\delta(d - d_0)$ is the Dirac delta function, and $\overline{f}_D(d)$ is the displacement probability density function for $D > d_0$. A mixed probability distribution has a finite probability at $D = d_0 = 0.5$ cm and a continuous probability density for $D > d_0$. The resulting model provides an equation for computing the probability of "zero" (i.e., negligible) displacement and an equation for computing the "nonzero" displacement.

The "zero" and "nonzero" displacement equations can be combined to calculate the probability of the seismic displacement exceeding a specified seismic slope displacement (d) for an earthquake scenario (i.e., $S_a(1.3T_s)$ and M_w) and slope properties (i.e., k_y and T_s). The probability of the seismic slope displacement (D) exceeding a specified displacement (d) is:

$$P(D > d) = [1 - P(D = 0)]P(D > d|D > 0) \tag{3}$$

where $P(D = 0)$ is computed using the probability of "zero" displacement equations that follow, and the term $P(D > d|D > 0)$ is computed assuming that the estimated displacements are lognormally distributed as:

$$P(D > d|D > 0) = 1 - P(D \le d|D > 0) = 1 - \Phi\left(\frac{Ln(d) - Ln(\widehat{d})}{\sigma}\right) \tag{4}$$

where $Ln(\widehat{d})$ is calculated using the "non-zero" equations that follow, and σ is the standard deviation of the random error of the applicable equation.

4.2. Shallow crustal earthquakes

A total of 6711 ground motion records (with each record having 2 horizontal components) from shallow crustal earthquakes along active plate margins were employed in the Bray and Macedo [24] update of the Bray and Travasarou [21] procedure. Their study took advantage of the NGA-West2 empirical ground motion database [25]. Each ground motion recording horizontal component was applied to the rigid base below the fully coupled, nonlinear, deformable stick-slip sliding block to calculate seismic displacement [24]. The seismic displacement values calculated from the two horizontal components were averaged for ordinary ground motions, which are ground motions without near-fault forward-directivity pulses. The opposite polarity of the horizontal components, which represents an alternative excitation of the slope, was also used to compute an alternative average seismic displacement, and the maximum of the average seismic displacement value for each polarity was assigned to that ground motion record. For the near-fault forward-directivity pulse motions, the two recorded orthogonal horizontal components for each recording were rotated from 0° to 180° in 1° increments for each polarity to identify the component producing the maximum seismic displacement (*D100*) and median seismic displacement (*D50*). Nearly 3 million sliding block analyses were performed in the [24] study.

In the near-fault region, the seismic slope displacement will be greatest for slopes oriented so their movement is in the fault-normal direction due to forward-directivity pulse motions. In this case, the *D100* equations developed by Ref. [24] should be used. If the slope is oriented so its movement is in the fault-parallel direction, the *D50* equations are used. *PGV* is required for near-fault motions in combination with $S_a(1.3T_s)$, which is the 5%-damped spectral acceleration at the degraded period of the sliding mass estimated as $1.3T_s$. The resulting *D100* equations are:

$$P(D100 = 0) = \left[1 + \exp\left(-10.787 - 8.717\,Ln(k_y) + 1.660\,Ln(PGV) + 3.150T_s + 7.560\,Ln(Sa(1.3T_s))\right)\right]^{-1} \text{ when } T_s \le 0.7 \text{ s} \tag{5a}$$

$$P(D100 = 0) = \left[1 + \exp\left(-12.771 - 9.979\,Ln(k_y) + 2.286\,Ln(PGV) - 4.965T_s + 4.817\,Ln(Sa(1.3T_s))\right)\right]^{-1} \text{ when } T_s > 0.7 \text{ s} \tag{5b}$$

$$Ln(D100) = c1 - 2.632\,Ln(k_y) - 0.278(Ln(k_y))^2 + 0.527\,Ln(k_y)Ln(Sa(1.3T_s)) + 1.978\,Ln(Sa(1.3T_s)) - 0.233(Ln(Sa(1.3T_s)))^2 + c2T_s + c3(T_s)^2 + 0.01M_w + c4 * Ln(PGV) \pm \varepsilon \tag{6}$$

where $P(D100 = 0)$ is the probability of occurrence of "zero" seismic slope displacement (as a decimal number); $D100$ is the "nonzero" maximum component seismic displacement in cm; k_y is the yield coefficient; T_s is the initial fundamental period of the sliding mass in seconds; and $S_a(1.3T_s)$ the spectral acceleration at a period of $1.3T_s$ in the units of g of the design outcropping ground motion for the site conditions below the potential sliding mass (i.e., the value of $S_a(1.3T_s)$ for the earthquake ground motion at the elevation of the sliding surface if the potential sliding mass was removed); ε is a normally distributed random variable with zero mean and standard deviation $\sigma = 0.56$. When $PGV \leq 150$ cm/s, $c1 = -6.951$, $c2 = 1.069$, $c3 = -0.498$, and $c4 = 1.547$ if $T_s \geq 0.10$ s, and $c1 = -6.724$, $c2 = -2.744$, $c3 = 0.0$, and $c4 = 1.547$ if $T_s < 0.10$ s. When $PGV > 150$ cm/s, $c1 = 1.764$, $c2 = 1.069$, $c3 = -0.498$, and $c4 = -0.097$ if $T_s \geq 0.10$ s, and $c1 = 1.991$, $c2 = -2.744$, $c3 = 0.0$, and $c4 = -0.097$ if $T_s < 0.10$ s. The $D50$ equations are:

$$P(D50=0) = \left[1 + \exp\left(-14.930 - 10.383\,Ln(k_y) + 1.971\,Ln(PGV) + 3.763T_s + 8.812\,Ln(Sa(1.3T_s))\right)\right]^{-1} \text{ when } T_s \leq 0.7 \text{ s} \quad (7a)$$

$$P(D50=0) = \left[1 + \exp\left(-14.671 - 10.489\,Ln(k_y) + 2.222\,Ln(PGV) - 4.759T_s + 5.549\,Ln(Sa(1.3T_s))\right)\right]^{-1} \text{ when } T_s > 0.7 \text{ s} \quad (7b)$$

$$Ln(D50) = c1 - 2.931\,Ln(k_y) - 0.319\left(Ln(k_y)\right)^2 + 0.584\,Ln(k_y)Ln(Sa(1.3T_s)) + 2.261\,Ln(Sa(1.3T_s)) - 0.241(Ln(Sa(1.3T_s)))^2 + c2T_s + c3(T_s)^2 + 0.05M_w + c4 * Ln(PGV) \pm \varepsilon \quad (8)$$

where $P(D50 = 0)$ is the probability of occurrence of "zero" seismic slope displacement (as a decimal number); $D50$ is the "nonzero" median component seismic displacement in cm; ε is a normally distributed random variable with zero mean and standard deviation $\sigma = 0.54$. When $PGV \leq 150$ cm/s, $c1 = -7.718$, $c2 = 1.031$, $c3 = -0.480$, and $c4 = 1.458$ if $T_s \geq 0.10$ s, and $c1 = -7.497$, $c2 = -2.731$, $c3 = 0.0$, and $c4 = 1.458$ if $T_s < 0.10$ s. If $PGV > 150$ cm/s, $c1 = -0.369$, $c2 = 1.031$, $c3 = -0.480$, and $c4 = 0.025$ if $T_s \geq 0.10$ s, and $c1 = 2.480$, $c2 = -2.731$, $c3 = 0.0$, and $c4 = 0.025$ if $T_s < 0.10$ s.

Ordinary (non-pulse) motions produce these equations:

$$P(D=0) = 1 - \Phi\left(-2.48 - 2.97\,Ln(k_y) - 0.12\left(Ln(k_y)\right)^2 - 0.72T_s\,Ln(k_y) + 1.70T_s + 2.78\,Ln(S_a(1.3T_s))\right) \text{ when } T_s \leq 0.7 \text{ s} \quad (9a)$$

$$P(D=0) = 1 - \Phi\left(-3.42 - 4.93\,Ln(k_y) - 0.30\left(Ln(k_y)\right)^2 - 0.35T_s\,Ln(k_y) - 0.62T_s + 2.86\,Ln(S_a(1.3T_s))\right) \text{ when } T_s > 0.7 \text{ s} \quad (9b)$$

$$Ln(D) = a1 - 2.482\,Ln(k_y) - 0.244\left(Ln(k_y)\right)^2 + 0.344\,Ln(k_y)Ln(Sa(1.3T_s)) + 2.649\,Ln(Sa(1.3T_s)) - 0.090(Ln(Sa(1.3T_s)))^2 + a2T_s + a3(T_s)^2 + 0.603M_w \pm \varepsilon \quad (10)$$

where $P(D = 0)$ is the probability of occurrence of "zero" seismic slope displacement (as a decimal number); Φ is the standard normal cumulative distribution function; D is the amount of "nonzero" seismic slope displacement in cm; k_y, T_s, $S_a(1.3T_s)$, and M_w are as defined previously, and ε is a normally distributed random variable with zero mean and standard deviation $\sigma = 0.72$. In Eq. (10), $a1 = -5.981$, $a2 = 3.223$, and $a3 = -0.945$ for systems with $T_s \geq 0.10$ s, and $a1 = -4.684$, $a2 = -9.471$, and $a3 = 0.0$ for $T_s < 0.10$ s. The change in parameters at $T_s = 0.10$ s reduces the bias in the residuals for very stiff slopes. For the special case of the Newmark rigid-sliding block where $T_s = 0.0$ s, the "nonzero" D (cm) is estimated as:

$$Ln(D) = -4.684 - 2.482\,Ln(k_y) - 0.244\left(Ln(k_y)\right)^2 + 0.344\,Ln(k_y)Ln(PGA) + 2.649\,Ln(PGA) - 0.090(Ln(PGA))^2 + 0.603M_w \pm \varepsilon \quad (11)$$

where PGA is the peak ground acceleration in the units of g of the input base ground motion, and k_y, M_w, and ε are as defined previously for Eq. (10). If there are important topographic effects to capture for localized shallow sliding, the input PGA value should be adjusted as discussed previously (i.e., 1.3 PGA_{1D} for moderately steep slopes, 1.5 PGA_{1D} for steep slopes, or 2.0 PGA_{1D} for the dam crest). For long, shallow potential sliding masses, lateral incoherence of ground shaking reduces the input PGA value employed in the analysis (e.g., 0.65 PGA_{1D} for moderately steep slopes, [37].

The "nonzero" seismic slope displacement equation for the entire ground motion database of ordinary and near-fault pulse motions can be used to calculate a seismic coefficient (k) consistent with a specified allowable calculated seismic slope displacement (D_a) for the general case when $PGV \leq 115$ cm/s [24]. The owner and engineer should select D_a (cm) to achieve the desired performance level and the percent exceedance of this displacement threshold (e.g., median displacement estimate for $\varepsilon = 0$ or 16% exceedance displacement estimate for $\varepsilon = \sigma = 0.74$) considering the consequences of unsatisfactory performance at displacement levels greater than this threshold. The seismic demand is defined in terms of $S_a(1.3T_s)$ of the input ground motion for the outcropping site condition below the sliding mass and M_w of the governing earthquake event. If this value of k is used in a pseudostatic slope stability analysis and the calculated $FS \geq 1.0$, then the selected percentile estimate of the seismic displacement will be less than or equal to D_a. The minimum value of the acceptable FS should not be greater than 1.0, because FS varies nonlinearly as a function of the reliability of the system, and the procedure is calibrated to $FS \geq 1.0$.

The effects of specifying the allowable displacement as well as the level of the seismic demand in terms of $S_a(1.3T_s)$ on the value of k are illustrated in Fig. 4. Allowable displacement values of 5 cm, 15 cm, 30 cm, and 50 cm are used to illustrate the dependence of k on the selected level of D_a for a M_w 7.0 earthquake. Results are also provided at the 30 cm allowable displacement level for a lower magnitude event ($M_w = 6$). As expected, k increases systematically as the 5%-damped elastic spectral acceleration of the ground motion increases. Importantly, k also increases systematically as the allowable displacement value decreases. It also decreases as the earthquake magnitude decreases. The seismic coefficient varies systematically in a reasonable manner as the allowable displacement threshold and design ground shaking level vary.

4.3. Interface and intraslab subduction zone earthquakes

Macedo et al. [34] recently updated the subduction zone interface earthquake seismic slope displacement procedure developed by Bray et al. [36]. They took advantage of the recently developed comprehensive NGA-Sub ground motion database [26] generated by the Pacific Earthquake Engineering Research (PEER) Center. Macedo et al. [34] utilized 6240 two-component horizontal ground motion recordings from 174 interface earthquakes with M_w from 4.8 to 9.1 to calculate seismic slope displacements with the Bray and Macedo [24] coupled nonlinear sliding block model.

An engineering-oriented robust seismic slope displacement developed using subduction zone intraslab earthquake ground motions did not exist. Given intraslab earthquake ground motion models differ from interface earthquake ground motion models, one should expect that the seismic slope displacement models for these two types of earthquakes to

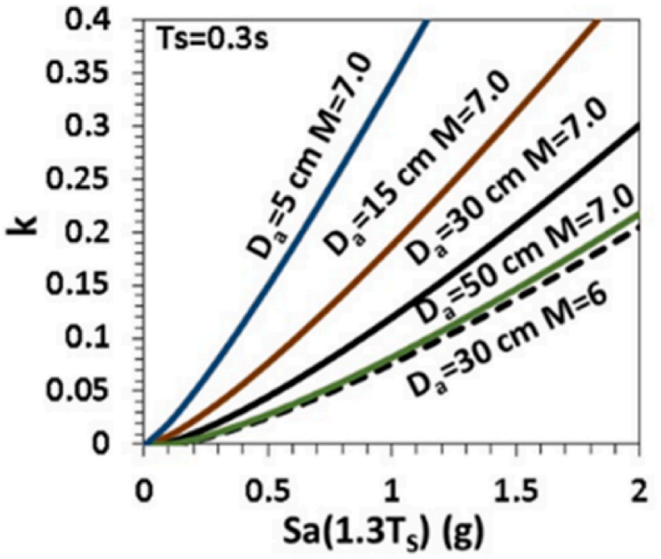

Fig. 4. Seismic coefficient as a function of the allowable displacement and seismic demand for ordinary and near-fault pulse motions when $PGV \leq 115$ cm/s.

differ. Macedo et al. [34] utilized 8299 two-component ground motion recordings from 200 intraslab earthquakes with M_w from 4.0 to 7.8 to calculate seismic slope displacements. They found there were significant biases in the residuals from the seismic slope displacements calculated using subduction zone interface seismic slope displacement models when comparing them with the displacements calculated using the intraslab earthquake records. Therefore, separate regressions were performed on the seismic slope displacements calculated using the interface and intraslab records.

As the two horizontal components of a ground motion record are highly correlated, the D value assigned to each two-component ground motion recording is the larger of the average displacement values calculated from the record's two polarities as was done for the shallow crustal ground motions in the [24] study. This methodology mirrors what is typically done in engineering practice. Over 1.5 million and 1.8 million analyses were performed using the interface and intraslab records, respectively.

A logistic regression [38] is the basis of the model to estimate $P(D = 0)$ as a function of k_y, T_s, and $S_a(1.3T_s)$ with the resulting equation of:

$$ln\frac{P(D=0)}{1-P(D=0)} = c_1 + c_2 \ln k_y + c_3 (\ln k_y)^2 + c_4 T_s \ln k_y + c_5 T_s + c_4 T_s lnSa(1.3T_s) \quad (12)$$

where c_1 to c_6 are coefficients provided in Table 2. The "nonzero" seismic displacement equation has a similar form to that used by Ref. [36] as follows:

$$lnD = a_0 + a_1 \ln k_y + a_2 (\ln k_y)^2 + a_3 \ln k_y lnSa(1.3T_s) + a_4 lnSa(1.3T_s) + a_5 (lnSa(1.5T_s)^2 + a_6 T_s + a_7 (T_s)^2 + a_8 M + \varepsilon \quad (13)$$

where a_0 to a_8 are model coefficients presented in Table 3, and ε is a Gaussian random variable with zero mean and standard deviation of $\sigma = 0.75$ for the interface event and $\sigma = 0.62$ for the intraslab event. The values of the coefficients a_0, a_6, and a_7 are modeled as dependent on the values of T_s based on residual analyses. The residuals show negligible bias and no significant trends for the seismic slope displacement models developed for interface and intraslab earthquakes for $PGV \leq 40$ cm/s and 20 cm/s for interface and intraslab earthquakes, respectively. The bias in estimating seismic slope displacement using Eq. (13) can be eliminated for cases with higher PGV values, and the overall standard deviation of the interface and intraslab earthquake models can be reduced to 0.65 and 0.53, respectively, by including PGV in a vector hazard model [34]. The addition of PGV in the models lowers the uncertainty of estimating seismic slope displacement given the inputs of the model are known, but the uncertainty in estimating the additional ground motion parameter of PGV increases the uncertainty in estimating the inputs to the seismic slope displacement model. The overall effect on the seismic slope displacement estimate depends on several factors, including the uncertainty in estimating PGV, the correlation between PGV and $S_a(1.3T_s)$, the shape of the hazard curve, and k_y.

Table 2
Coefficients for interface and intraslab earthquakes $P(D = 0)$ equations.

Coefficient	Interface	Intraslab
c_1	3.46 for $T_s < 0.6$; 3.57 for $T_s \geq 0.6$	5.22 for $T_s < 0.6$; 2.92 for $T_s \geq 0.6$
c_2	5.05 for $T_s < 0.6$; 9.39 for $T_s \geq 0.6$	6.55 for $T_s < 0.6$; 14.72 for $T_s \geq 0.6$
c_3	0.15 for $T_s < 0.6$; 0.55 for $T_s \geq 0.6$	0.43 for $T_s < 0.6$; 2.24 for $T_s \geq 0.6$
c_4	1.41 for $T_s < 0.6$; 1.64 for $T_s \geq 0.6$	4.73 for $T_s < 0.6$; 5.45 for $T_s \geq 0.6$
c_5	−1.08 for $T_s < 0.6$; 5.37 for $T_s \geq 0.6$	−0.87 for $T_s < 0.6$; 14.82 for $T_s \geq 0.6$
c_6	−5.13 for $T_s < 0.6$; −7.00 for $T_s \geq 0.6$	−6.50 for $T_s < 0.6$; −8.47 for $T_s \geq 0.6$

Table 3
Coefficients for interface and intraslab earthquakes 'nonzero" D equations.

Coefficient	Interface	Intraslab
a_0	−5.00 for $T_s < 0.1$; −6.19 for $T_s \geq 0.1$	−4.13 for $T_s < 0.1$; −5.27 for $T_s \geq 0.1$
a_1	−3.18	−2.21
a_2	−0.35	−0.20
a_3	0.45	0.22
a_4	2.89	2.31
a_5	−0.14	−0.02
a_6	−9.46 for $T_s < 0.1$; 2.87 for $T_s \geq 0.1$	−9.45 for $T_s < 0.1$; 3.63 for $T_s \geq 0.1$
a_7	0 for $T_s < 0.1$; −0.86 for $T_s \geq 0.1$	0 for $T_s < 0.1$; −1.10 for $T_s \geq 0.1$
a_8	0.46	0.50

The Macedo et al. [34] interface model produces seismic slope displacements consistent with the Bray et al. [36] interface earthquake model. However, the Macedo et al. [34] intraslab model produces significantly different results than the interface models (a comparison with [36] interface model is shown in Fig. 5). Most of the coefficients in the seismic slope displacement equations developed by Ref. [34] for subduction zone interface earthquakes and intraslab earthquakes differ significantly, which highlights the different scaling of seismic slope displacement for these different types of earthquake sources. In addition, the standard deviation of the intraslab model is smaller than that of the interface model.

5. Seismic slope displacement hazard

5.1. Background

The seismic slope displacement models discussed in previous sections can be used in performance-based probabilistic assessments that capture uncertainties of the ground motion models and slope properties (e.g., Ref. [39]; and [40]). The aleatory uncertainty in estimating the seismic slope displacement can be captured through integration of the distribution of the random variables in the hazard calculation. The epistemic uncertainty of the slope properties (i.e., k_y and T_s) can be addressed using logic trees. The outcome of these assessments is a seismic slope displacement hazard curve, which relates different displacement thresholds with their annual rate of exceedance.

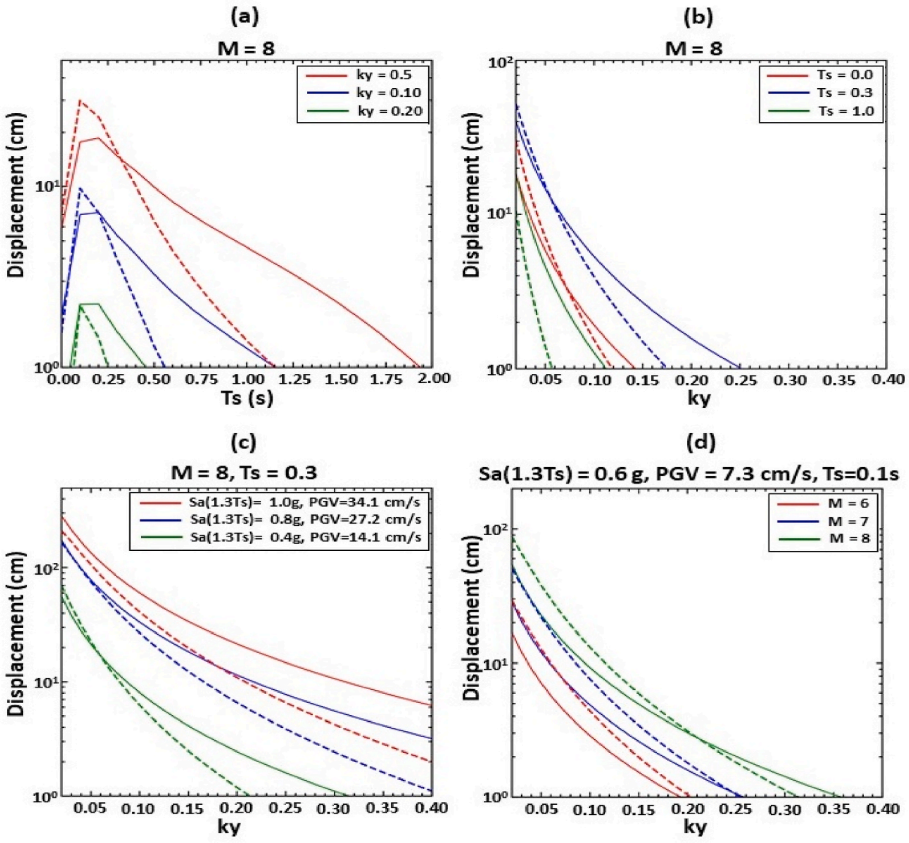

Fig. 5. Comparison of the [34] intraslab model (solid curves) with the [36] interface model (dashed curves) with variations in k_y, T_s, $Sa(1.3T_s)$, PGV, and M.

Displacement hazard curves are calculated as [41]:

$$\lambda_D(z) = \sum_{i=1}^{nk_y} \sum_{j=1}^{nT_s} \times \int_{M_{min}}^{M_{max}} \int_{IM} w_i w_j P\left(D > z | IM, M, k_y^i, T_s^j\right) P(M|IM) \Delta\lambda(IM) d(IM) d(M) \tag{14}$$

where D represents the slope displacement, IM can be a scalar or a vector of ground motion intensity measures (i.e., $Sa(1.3T_s)$ or PGV), and $\lambda_D(z)$ is the mean annual rate slope displacement exceeding a given threshold z. Also, $\Delta\lambda(IM)$ is the joint annual rate of occurrence of IM and $P(M|IM)$ is the conditional probability of M given IM, which can be estimated from a probabilistic seismic hazard assessment (PSHA). nk_y and nT_s are the number of different k_y and T_s values considered for the slope system to account for the uncertainty in the slope properties. k_y^i and T_s^j are the i-th and j-th realizations of k_y and T_s with weighting factors w_i and w_j, respectively. $P(D > z|IM, M, k_y^i, T_s^j)$ is the conditional probability of D exceeding z given the values of IM, M, k_y^i and T_s^j, which can be estimated as:

$$\begin{aligned} P(D > z) &= \left(1 - P\left(D = 0 | IM, M, k_y^i, T_s^j\right)\right) P(D > z | D > 0) \\ &= \left(1 - P\left(D = 0 | IM, M, k_y^i, T_s^j\right)\right) (1 - P(D \le z | D > 0)) \\ &= \left(1 - P\left(D = 0 | IM, M, k_y^i, T_s^j\right)\right) \left(1 - \Phi\left(\frac{lnz - ln\,\mu\left(IM, M, k_y^i, T_s^j\right)}{\sigma}\right)\right) \end{aligned} \tag{15}$$

where Φ is the cumulative distribution function of the standard normal distribution and $\mu(IM, M, k_y^i, T_s^j)$ and σ are the median value and standard deviation of D, which can be estimated using slope displacement models given IM, M, T_s and k_y. $P(D = 0)$ can be estimated using equations that provide the probability of "zero" displacement. Note Eq. (14) can be applied separately to different tectonic settings. For instance, when considering the subduction interface, subduction intraslab, and shallow crustal settings, three different annual rate of exceedance curves can be evaluated for each tectonic setting ($\lambda_D^{interface}$, $\lambda_D^{intraslab}$, and $\lambda_D^{crustal}$) by using the corresponding deaggregated ground motion hazard, which can be combined to estimate the total annual rate of exceedance λ_D^{total} as:

$$\lambda_D^{total} = \lambda_D^{interface} + \lambda_D^{intraslab} + \lambda_D^{crustal} \tag{16}$$

In addition to providing the total seismic slope displacement hazard, Equation (16) also enables deaggregation of the contribution of different tectonic mechanisms to the total hazard, which is a feature commonly used in PSHA. Deaggregation of the total hazard provides valuable insights into assessing the seismic slope displacement hazard. For instance, Fig. 6 shows an example of seismic hazard curves for the seismic intensity parameter S_a and the seismic slope displacement hazard curves estimated by Ref. [41] for a site near Seattle, Washington with contributions from subduction interface, subduction intraslab, and shallow crustal sources. Interestingly, from the PSHA results in terms of S_a shown in Fig. 6a, it is apparent that shallow crustal sources contribute the most to the seismic hazard. However, the seismic slope displacement hazard curves shown in Fig. 6b show that the interface seismic sources contribute most to the seismic slope displacement hazard. In this example, giving more weight to shallow crustal sources in the selection of ground motions based on the PHSA is misleading as the seismic performance of a slope system is more directly related to seismic slope displacement than S_a. Hence, the interface seismic zone should receive more weight.

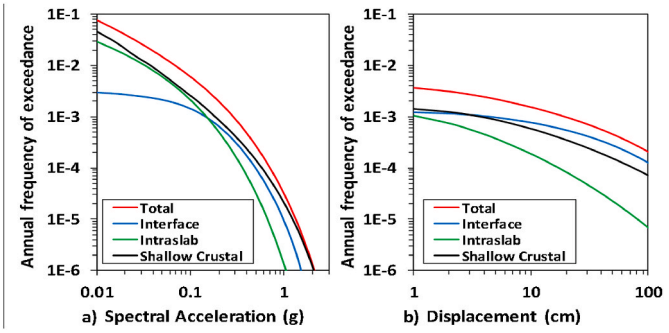

Fig. 6. Differences between a) spectral acceleration hazard curves at $1.5T_s$ = 1.0 s and b) seismic slope displacement hazard curves for site near Seattle, Washington.

The estimation of seismic slope displacement (D) hazard curves can also be used to deaggregate earthquake scenarios (i.e., magnitude and distance) that contribute the most to the D hazard. Considering a combination of nM magnitudes, nR site-to-source distances, and $n\varepsilon$ epsilon values (i.e., the number of standard deviations above the median intensity measure estimate), the total number of scenarios would be $nScen = nM * nR * n\varepsilon$. In addition, considering nx intensity measure levels and ny levels of D; the intensity measure hazard can be stored in a matrix $\lambda(IMT)$ of size $nScen$ by nx. For a fixed D level, k_y, and T_s values, Eq. (14) can be evaluated for each ground motion scenario and intensity measure level, resulting in a matrix $PS\lambda_D$, which contains the partial annual rate of exceedance sorted by scenarios and intensity measure values. The D hazard contribution from all intensity measure levels can be computed by summing up all columns of $PS\lambda_D$, resulting in a vector $S\lambda_D = [S\lambda_D^1,\ldots,S\lambda_D^{nScen}]$, this vector can be used as a proxy to perform the deaggregation of hazard curves as follows (see Ref. [41]:

$$DeaggD_j = S\lambda_{D_j}^i \Big/ \sum_{p=1}^{nScen} S\lambda_{D_j}^p \quad \text{for } j = 1 : ny \tag{17}$$

where $DeaggD_j$ contains the earthquake scenarios deaggregated for the jth D level.

Previous studies that considered performance-based probabilistic assessments have often focused on one tectonic setting (e.g., shallow crustal) and considered simplified seismic sources. In contrast, the recent developments conducted by the authors are focused on incorporating realistic seismic sources (i.e., representative of realistic project scenarios) and multiple tectonic settings, which is a step forward in engineering practice. In particular, the Macedo et al. [34] model for intraslab settings has not been previously implemented within a performance-based probabilistic framework. It is worth highlighting that Macedo and Candia [42] modified the procedures described in this section to estimate hazard-consistent seismic coefficients for pseudo-static analyses. Computational tools to use these methods have been implemented by Ref. [41] to facilitate their use in practice.

5.2. Seismic slope displacement hazard example

Consider the hypothetical 57-m high earth dam founded on bedrock shown in Fig. 7, which is hypothetically located in the Peruvian Andes in an area affected by earthquakes from multiple tectonic settings (i.e., shallow crustal and subduction zone interface and intraslab earthquakes). The T_s, and k_y values for the dam are 0.33 s and 0.14, respectively. T_s is estimated based on the measured shear wave velocities considering V_s = 400 m/s and k_y is estimated using pseudo-static slope stability analyses ([21] provide additional details). The uncertainties in k_y and T_s, which can be handled in performance-based probabilistic assessments, have been considered through the coefficients of variations (COV) of k_y (COV = 0.25) and T_s (COV = 0.15) assuming their distributions are lognormal, with weights estimated as recommended by Ref. [40] in which the weights of different k_y values are normalized based on their amplitudes in a lognormal distribution. A potential correlation between k_y and T_s was not considered in this example. Additional research is required to assess potential correlations. The assessment is performed for the critical sliding surface, which is a deep sliding surface near the base of the dam.

The seismic slope displacement hazard assessment is conducted using the displacement models developed by Ref. [34] for subduction zones (considering the models with two intensity measures, i.e., $Sa(1.3T_s)$ and PGV) and the model developed by Ref. [36] for interface subduction zones. In addition, the Bray and Macedo [24] displacement model for shallow crustal earthquake zones is used. The Macedo et al. [34] subduction interface model is weighted 0.6, whereas the Bray et al. [36] model is weighted 0.4 for subduction interface earthquakes. The Bray and Macedo [24] shallow crustal model and the Macedo et al. [34] subduction intraslab model are used with a weight of 1.0 for these cases. Only one seismic slope displacement model was considered for shallow crustal earthquakes in this example, which is appropriate for the site in the Peruvian Andes because its seismic hazard is governed by subduction zone earthquakes. If a significant contribution from shallow crustal seismic sources is expected, several shallow crustal earthquake seismic slope displacement models should be used. Additionally, several seismic slope displacement models for subduction zone earthquakes should be included in the hazard assessment as additional robust subduction zone earthquake models become available.

First, a PSHA assessment is conducted, which requires different GMMs. Specifically, the results shown in Fig. 8a and b consider the GMMs for $Sa(1.3T_s)$ and PGV from Kuehn et al. (2020 – KBCG), Parker et al. (2020 – PSHAB), and Candia et al. (2020 – SiberRisk) weighted equally in the case of subduction interface and subduction intraslab earthquake zones; whereas the GMMs from the NGAWest2 project (i.e., Abrahamson et al., 2014 – ASK14; Boore et al., 2014 – BSSA14; Chiou and Youngs. 2014 – CY14; and Campbell and Bozorgnia 2014 – CB14) are weighted equally for shallow crustal settings. Because the seismic slope displacement models for subduction zones use two intensity measures ($Sa(1.3T_s)$ and PGV), their coefficient of correlation is required to estimate their joint rate of occurrence, which is an input into the ground motion hazard used to compute a seismic slope displacement hazard curve. Engineers can use the coefficients of correlation in Ref. [43] for shallow crustal settings and those in Ref. [44] for subduction earthquake zones.

Uncertainties in slope properties can also be incorporated using logic trees (e.g., Ref. [40]. This assessment considers 9 realizations for T_s (0.25 s–0.41 s, with a best estimate of 0.33 s) and k_y (0.11–0.18, with a best estimate of 0.14). The considered values consider an equal partition in the log space. The weights for each realization (i.e., 0.3, 0.4, and 0.3 for k_y and T_s) are assigned as per [40]; as discussed previously and are shown in Table 4 to capture these aspects of epistemic uncertainty.

Fig. 9 shows the seismic slope displacement hazard curves developed in this assessment. Fig. 9a shows the mean hazard curves, 5–95 percentiles, and individual realizations, whereas Fig. 9b shows the displacement hazard deaggregation by tectonic settings. For this earth dam at this site, the intraslab seismic sources largely control the seismic slope displacement hazard. The interface seismic sources are of secondary importance, and the contribution from shallow crustal source is less important. This example highlights the potential importance of intraslab tectonic settings in the performance-based seismic assessments of slope systems in similar tectonic settings.

The seismic slope displacement hazard curves shown in Fig. 9a provide hazard-consistent estimates. One does not need to assume the hazard level for seismic slope displacement is the same as that for a particular ground motion intensity measure, which is an implicit assumption often made in seismic performance assessments of slopes. Seismic slope displacements at the 475 and 2475 years return period are

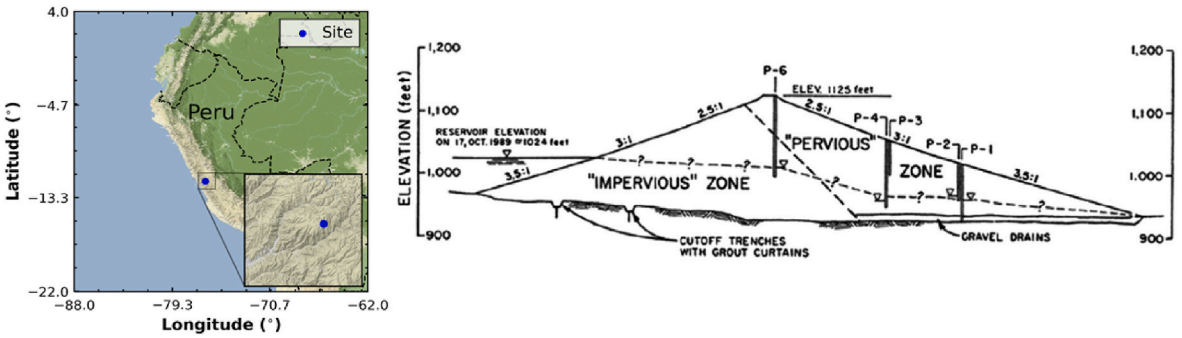

Fig. 7. Illustrative performance-based probabilistic assessment of a hypothetical earth dam in the Peruvian Andes.

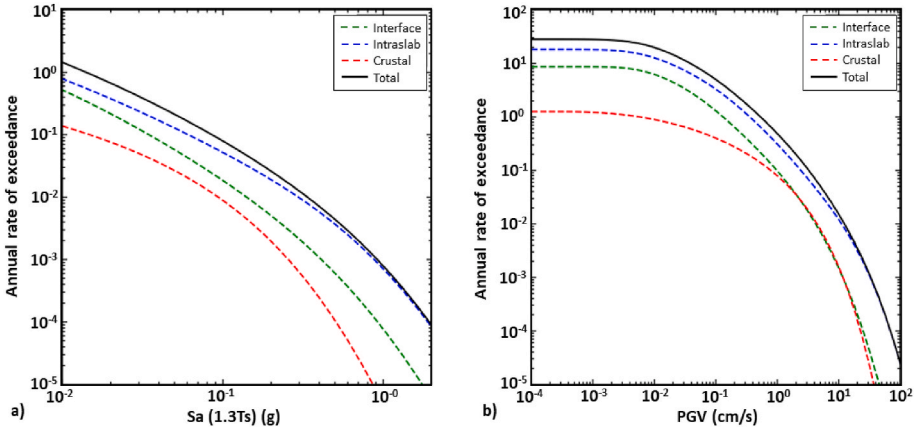

Fig. 8. Performance-based probabilistic assessment of a hypothetical earth dam in the Peruvian Andes. Deaggregation of (a) $Sa(1.3T_s)$ and (b) *PGV* hazard curves by tectonic mechanism.

Table 4
Performance-based probabilistic assessment of a slope system in Peru. Weights for slope properties.

Slope Parameters		
T_s	k_y	Weight
0.248	0.105	0.09
0.248	0.140	0.12
0.248	0.175	0.09
0.330	0.105	0.12
0.330	0.140	0.16
0.330	0.175	0.12
0.413	0.105	0.09
0.413	0.140	0.12
0.413	0.175	0.09

estimated directly as 8 cm and 27 cm, respectively (Fig. 9a).

Lastly, this performance-based probabilistic procedure enables the seismic slope displacement hazard to be deaggregated using Eq. (17). The mean displacement hazard curve shown in Fig. 9 is deaggregated at the 475 and 2475 year of return periods in terms of distance and magnitude as shown in Fig. 10. The deaggregation indicates that the displacement hazard is controlled by intraslab earthquakes with magnitudes between 7.8 and 8.2 and distances between 90 and 110 km. The deaggregation directly from the seismic slope displacement hazard provides guidance regarding the selection of design ground motions for this project as opposed to using the results of a PSHA based only on a ground motion intensity measure.

6. Conclusions

In evaluating seismic slope stability, the engineer must first determine if there are materials in the system or its foundation that will lose significant strength due to cyclic loading. If there are materials that can lose significant strength, post-cyclic reduced strengths should be employed in a static slope stability analysis to calculate the post-cyclic *FS*. If it is low, this issue should be the primary focus of the evaluation because a flow slide could occur. If materials will not lose significant strength due to cyclic loading, the deformation of the earth structure or slope should be evaluated to assess if it is sufficient to jeopardize satisfactory performance of the system.

A modified Newmark model with a deformable sliding mass provides useful insights for estimating seismic slope displacement due to shear deformation of the earth materials comprising earth dams and natural slopes for the latter case discussed above. The critical components of a sliding block analysis are: 1) the dynamic resistance of the structure, 2) the earthquake ground motion, 3) the dynamic response of the potential sliding mass, and 4) the permanent displacement calculational procedure. Seismic slope displacement procedures should be evaluated in terms of how each procedure characterizes the slope's dynamic resistance, earthquake ground motion, dynamic response of the system, and calculational procedure.

The system's dynamic resistance is captured by its yield coefficient. This important system property depends greatly on the shear strength of the soil along the critical sliding surface. Assessment of the dynamic peak shear strength of a clay material requires consideration of the rate of loading, cyclic degradation, progressive failure, and distributed shear deformation effects. If the clay exhibits strain-softening and moderate-to-large displacements are calculated, the k_y value used in the sliding block analysis must be compatible with the reduction in clay shear

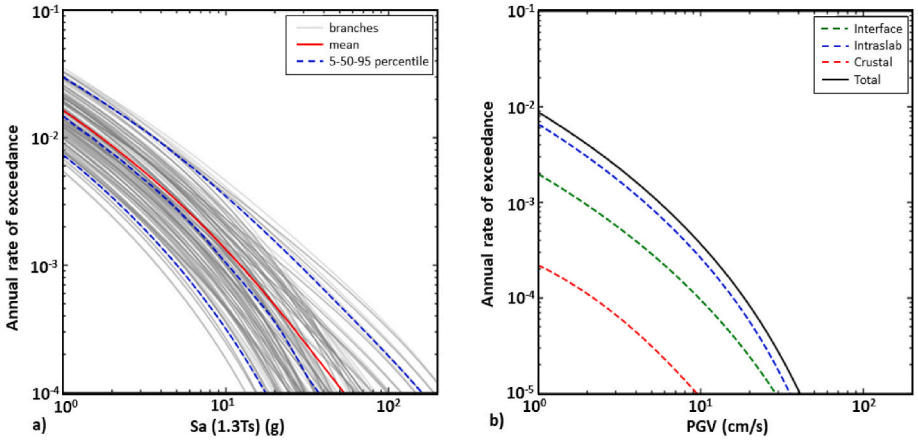

Fig. 9. Performance-based probabilistic assessment of a hypothetical earth dam in the Peruvian Andes: (a) seismic slope displacement hazard curves, and (b) deaggregation of displacement hazard by tectonic mechanisms.

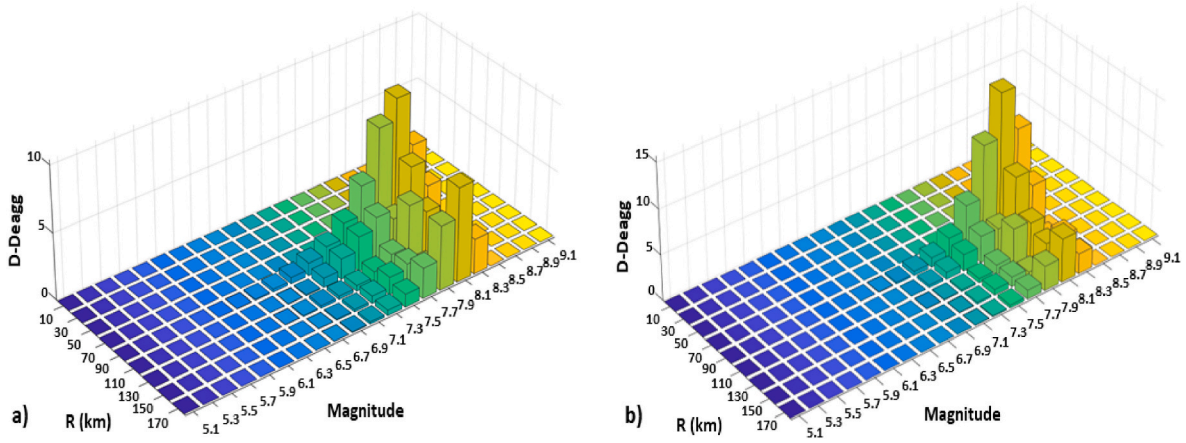

Fig. 10. Performance-based probabilistic assessment of a hypothetical earth dam in the Peruvian Andes. Earthquake scenario deaggregation from seismic slope displacement hazard curve at return periods of (a) 475 and (b) 2475 years.

strength with increasing displacement.

The primary source of uncertainty in assessing the seismic performance of an earth slope when there are no materials that can undergo severe strength loss is the input ground motion. Recent models have taken advantage of the wealth of strong motion records that are now available. The Bray and Macedo and the Macedo et al. [24,34] procedures are based on the results of coupled nonlinear deformable stick-slip sliding block analyses using large databases of thousands of recorded ground motions. Their model captures shear-induced displacement due to sliding on a distinct plane and distributed shear shearing within the slide mass.

The spectral acceleration of the ground beneath a potential sliding mass at a degraded period of the sliding mass ($S_a(1.3T_s)$) is an optimal ground motion intensity measure. As it only captures the intensity and frequency content of the ground motion, M_w is added as a proxy to represent the important effect of duration. In some cases, the addition of *PGV* is necessary to minimize bias and reduce the scatter in the residuals. *PGV* is especially informative when applying the Bray and Macedo [24] model to estimate seismic displacement for slopes with movement oriented in the fault-normal direction in the near-fault region. Forward-directivity velocity pulse motions tend to produce a large seismic slope displacement in the fault normal direction, captured by *D100*, which is systematically greater than the median component of motion (*D50*).

The Bray and Macedo and Macedo et al. [24,34] procedures use a mixed random variable formulation to separate the probability of "zero" displacement (i.e., ≤0.5 cm) occurring from the distribution of "nonzero" displacement, so that very low values of calculated displacement that are not of engineering interest do not bias the results. The calculation of the probability of "zero" displacement occurring provides a screening assessment of seismic performance. If the likelihood of negligible displacements occurring is not high, the "nonzero" displacement is estimated. The 16%–84% exceedance seismic displacement range should be estimated as there is considerable uncertainty in the estimate of seismic slope displacement. This displacement range is approximately half-to-twice the median seismic displacement estimate.

These procedures provide estimates of seismic slope displacement that are generally consistent with documented cases of earth dam and solid-waste landfill performance for shallow crustal earthquakes and subduction zone earthquakes. The proposed models can be used in a deterministic analysis or they can be implemented rigorously within a fully probabilistic framework to evaluate the seismic slope displacement hazard. We recommend moving towards performance-based probabilistic approaches because they provide hazard-consistent estimates of seismic slope displacement, which do not rely on the assumption that the ground motion intensity measure and displacement hazard levels are identical. This commonly held assumption is not true in many cases. Moreover, performance-based probabilistic assessments provide a framework for better treatment of uncertainties and can also be extended to the estimation of seismic coefficients for pseudostatic analyses. Lastly, it is important to emphasize the estimated range of seismic slope displacement is an index of the likely seismic performance of the

earth slope.

The updated seismic slope displacement models discussed in this study are provided in the form of a spreadsheet at: http://www.ce.berkeley.edu/people/faculty/bray/research.

CRediT authorship contribution statement

Jonathan D. Bray: Conceptualization, Methodology, Writing – original draft, Project administration, Funding acquisition. **Jorge Macedo:** Conceptualization, Methodology, Writing – review & editing, Funding acquisition.

Declaration of competing interest

The authors declare that they have no known competing financial interests or personal relationships that could have appeared to influence the work reported in this paper.

Data availability

No data was used for the research described in the article.

Acknowledgements

The Faculty Chair in Earthquake Engineering Excellence at UC Berkeley provided financial support to perform this research, which was supplemented by Georgia Tech. The PEER Center provided access to the NGA-West2 and NGA-Sub intensity measures.

References

[1] Newmark NM. Effects of earthquakes on dams and embankments. *Geotechnique*, London 1965;15(2):139–60.
[2] Bray JD, Frost JD, editors. Geo-engineering reconnaissance of the 2010 Maule, Chile earthquake, a report of the NSF- sponsored GEER association team; 2010. http://www.geerassociation.org/.
[3] Stewart JP, Bray JD, McMahon DJ, Smith PM, Kropp AL. Seismic performance of hillside fills. J Geotech Geoenviron Eng 2001;V127(11):905–19.
[4] Tokimatsu K. Seed, H.B.: evaluation of settlements in sands due to earthquake shaking. J. Geotech. Engrg., ASCE, V. 1987;113(8):861–78.
[5] Blake TF, Hollingsworth RA, Stewart JP, editors. Recommended procedures for implementation of DMG special publication 117 guidelines for analyzing and mitigating landslide hazards in California. June.: Southern California Earthquake Center; 2002.
[6] Holtz RD, Kovacs WD, Sheahan TC. An introduction to geotechnical engineering. second ed. Upper Saddle River, NJ: Prentice Hall; 2011.
[7] Duncan JM, Wright SG, Brandon TL. Soil strength and slope stability. second ed. NJ: John Wiley & Sons; 2014.
[8] Chen WY. Physical studies of seismic slope response and performance. Ph.D. Thesis. Univ. of Calif. Berkeley; 2004. December.
[9] Chen WY, Bray JD, Seed RB. Shaking table model experiments to assess seismic slope deformation analysis procedures. In: Proc. 8th US nat. Conf. EQ engrg., EERI; 2006. Paper 1322.
[10] Seed HB, Chan CK. Clay strength under earthquake loading condition. ASCE J Soil Mech Found Div 1966;92. No. SM, 2.
[11] Lacerda WJ. Sress relaxation and creep effects on the deformation of soils. Ph.D. Thesis. Berkeley: Univ. of California; 1976.
[12] Biscontin G, Pestana JM. Influence of peripheral velocity on undrained shear strength and deformability characteristics of a bentonite-kaolinite mixture. In: Geotech. Engrg. Report No. UCB/GT/99-19. Univ. of Calif. Berkeley, Revised December; 2000.
[13] Rau GA. Evaluation of strength degradation in seismic loading of embankments on cohesive soils. Ph.D. Thesis. December: Univ. of Calif. Berkeley; 1998.
[14] Kammerer AM, Hunt C, Riemer M. UC Berkeley geotechnical testing for the east Bay crossing of the san francisco-oakland Bridge, geotech. Engrg. Report No. UCB/GT/99-18, October. Univ. of Calif. Berkeley; 1999.
[15] Vucetic M. Cyclic threshold shear strains in soils. *J. Geotech. Engrg.*, ASCE, V. 1994;120(12):2208–28.
[16] Rumpelt TK, Sitar N. Simple shear tests on Bay Mud from borehole GT-2 S-2: richmond sanitary landfill, & the effect of the rate of cyclic loading in simple shear tests on san Francisco Bay Mud, reports for EMCON ASSOC., nov. 4 and dec. 13. 1988.
[17] Matasovic, N., Kavazanjian, Jr., E., Giroud, J.P., Newark seismic deformation analysis for geosynthetic covers. *Geosynth Int* V 5(1–2), 237-264.
[18] Duncan JM. State of the art: limit equilibrium and finite element analysis of slopes," ASCE. J Geotech Engrg 1996;122(7):577–96.
[19] Makdisi F, Seed HB. Simplified procedure for estimating dam and embankment earthquake-induced deformations. J Geotech Engrg., ASCE, V 1978;104(7):849–67.
[20] Seed HB, Martin GR. The seismic coefficient in earth dam design. J Soil Mech. Found. Div., ASCE, V 1966;92(3):25–58.
[21] Bray JD, Travasarou T. Simplified procedure for estimating earthquake-induced deviatoric slope displacements. J Geotech Geoenviron Eng 2007;133(4):381–92.
[22] Cornell C, Luco N. Ground motion intensity measures for structural performance assessment at near-fault sites," Proc. U.S.-Japan joint workshop and third grantees meeting. U.S.-Japan Coop. Res. On Urban EQ. Disaster Mitigation, Seattle, Washington. 2001.
[23] Rathje EM, Antonakos G. A unified model for predicting earthquake-induced sliding displacements of rigid and flexible slopes. Eng Geol 2011;122(1–2):51–60.
[24] Bray JD, Macedo J. Procedure for estimating shear-induced seismic slope displacement for shallow crustal earthquakes. J Geotech Geoenviron Eng 2019;145(12):04019106.
[25] Bozorgnia Y, Abrahamson NA, et al. NGA-West2 research project. *Earthq Spectra* V 2014;30(3):973–87. https://doi.org/10.1193/072113EQS209M.
[26] Bozorgnia Y, Abrahamson NA, Ahdi SD, et al. NGA-subduction research program. *Earthq Spectra* V 2021;38(2):783–98. https://doi.org/10.1177/87552930211056081.
[27] Kramer SL, Smith MW. Modified Newmark model for seismic displacements of compliant slopes. J Geot Geoenv Engrg., ASCE 1997;123(7):635–44.
[28] Rathje EM, Bray JD. Nonlinear coupled seismic sliding analysis of earth structures. J Geotech Geoenviron Eng 2000;126(11):1002–14.
[29] Wartman J, Bray JD, Seed RB. Inclined plane studies of the newmark sliding block procedure. J Geotech Geoenviron Eng 2003;129(8):673–84.
[30] Bray JD. Chapter 14: simplified seismic slope displacement procedures, *earthquake geotechnical engineering*, 4th int conf EQ geo eng. In: Pitilakis KD, editor. Geotechnical, geological, and earthquake engineering series, V6. Springer; 2007. p. 327–53.
[31] Bray JD, Macedo J. Closure to: procedure for estimating shear-induced seismic slope displacement for shallow crustal earthquakes. J Geotech Geoenviron Eng 2021. 10.1061/(ASCE)GT.1943-5606.0002143.
[32] Ambraseys NN, Sarma SK. The response of earth dams to strong earthquakes. *Geotechnique* V 1967;17:181–213.
[33] Yu L, Kong X, Xu B. Seismic response characteristics of earth and rockfill dams. Sept. Lisbon, Portugal: 15th WCEE; 2012. Paper No.2563.
[34] Macedo J, Bray JD, Liu C. Seismic slope displacement procedure for interface and intraslab subduction zone earthquakes. J Geotech Engrg 2023.
[35] Saygili G, Rathje EM. Empirical predictive models for earthquake-induced sliding displacements of slopes. J Geotech Geoenviron Eng 2008;134(6):790–803.
[36] Bray JD, Macedo J, Travasarou T. Simplified procedure for estimating seismic slope displacements for subduction zone earthquakes. J Geotech Geoenviron Eng 2018;144(3):04017124.
[37] Rathje EM, Bray JD. One- and two-dimensional seismic analysis of solid-waste landfills. Can Geotech J 2001;384:850–62.
[38] Hosmer Jr DW, Lemeshow S, Sturdivant RX. Applied logistic regression, vol. 398. John Wiley & Sons; 2013.
[39] Rathje EM, Saygili G. Pseudo-probabilistic versus fully probabilistic estimates of sliding displacements of slopes. J Geotech Geoenviron Eng 2011;137(3):208–17.
[40] Macedo J, Bray JD, Abrahamson N, Travasarou T. Performance-based probabilistic seismic slope displacement procedure. Earthq Spectra 2018;34(2):673–95.
[41] Macedo J, Candia G, Lacour M, Liu C. New developments for the performance-based assessment of seismically-induced slope displacements. Eng Geol J 2020;277:105786.
[42] Macedo J, Candia G. Performance-based assessment of the seismic pseudo-static coefficient used in slope stability analysis. Soil Dynam Earthq Eng 2020;133:106109.
[43] Baker JW, Bradley BA. Intensity measure correlations observed in the NGA-west2 database, and dependence of correlations on rupture and site parameters. Earthq Spectra 2017;33(1):145–56.
[44] Macedo J, Liu C. Ground-motion intensity measure correlations on interface and intraslab subduction zone earthquakes using the nga-sub database. Bull Seismol Soc Am 2021;111(3):1529–41.
[51] Wartman J, Seed RB, Bray JD. Shaking table modeling of seismically induced deformation in slopes. J Geotech Geoenviron Eng 2005;131(5):610–22.
[52] Jibson RW. Regression models for estimating coseismic landslide displacement. Eng Geo 2007;91(2–4):209–18. https://doi.org/10.1016/j.engeo.2007.01.013.
[53] Lin JS, Whitman RV. Decoupling approximation to the evaluation of earthquake-induced plastic slip in earth dams. EESD 1983 1983;11(5):667–78. https://doi.org/10.1002/eqe.4290110506.